ISSN 1330-3651 (Print), ISSN 1848-6339 (Online) https://doi.org/10.17559/TV-20230510000617
Original scientific paper

Auto-Alignment Non-Contact Optical Measurement Method for Quantifying Wobble Error of a Theodolite on a Vehicle-Mounted Platform

Xiangyu LI, Wei HAO, Meilin XIE, Bo LIU, Bo JIANG, Tao LV, Wei SONG, Ping RUAN*

Abstract: During non-landing measurements of a theodolite, the accuracy of the goniometric readings can be compromised by wobble errors induced by various factors such as wind loads, theodolite driving torque, and the stiffness of the supporting structure. To achieve high-precision non-landing measurements, it is essential to accurately determine and correct the platform wobble errors affecting the azimuth and pitch pointing angles. In this paper, a non-contact optical measurement method is proposed for quantifying platform wobble errors. The method establishes an auto-alignment optical path between an autocollimator and a reflector in the measuring device. By detecting the deviation angle of the CCD image point as the optical path changes, precise measurements of the platform wobble errors can be obtained. Experimental results demonstrate that the measuring device can achieve an auto-alignment optical path within 5 minutes, significantly improving measurement efficiency. Furthermore, after measuring the platform wobble error and applying data correction, the average error in the azimuth pointing angle is reduced from 31.5" to 9.8", and the average error in the pitch pointing angle is reduced from 21" to 9.2". These results highlight the substantial correction effect achieved by the proposed method.

Keywords: autocollimator; dual-axis inclinometer; electro-optical theodolite; optical measurement; vehicle-mounted platform; wobble error

1 INTRODUCTION

Electro-optical theodolites are mainly used to record the parameters of the target trajectory, flight attitude and radiation characteristics [1, 2]. In recent years, electro-optical theodolites have made considerable progress in application fields, tracking control algorithm and observation capabilities [3-13]. At the same time, the measurement method has also undergone important changes, gradually changing from a fixed foundation measurement mode into a vehicle-mounted measurement mode. Before the non-landing measurement of a vehicle-mounted theodolite, the theodolite generally needs to be supported by hydraulic or mechanical legs to disengage flexible links, such as tires. In the meantime, theodolite levelling, point positioning and azimuth/pitch pointing angle initialization also need to be completed. Compared to fixed-type theodolites, vehicle-mounted theodolites have the characteristics of fast unfolding, fast withdrawal and fast measuring [14, 15]. However, the vehicle-mounted platform for supporting the theodolite usually produces wobble errors that are induced by various factors such as wind loads, theodolite driving torque, and the stiffness of the supporting structure [16, 17]. Then, the wobble errors in turn affect the accuracy of the goniometric readings. Therefore, to achieve high-precision non-landing measurement of the theodolite, the platform wobble errors usually need to be obtained precisely for correction of the azimuth and pitch pointing angle [18-22].

Luo et al. [23, 24] presented a vehicle-mounted platform deformation measurement method using inertial sensors. The attitude measuring device is composed of a gyroscope and a dual-axis inclinometer. The gyroscope is used for twist angle measurement. The dual-axis inclinometer is used for roll angle and pitch angle measurements. Inertial sensors use gravity and earth rotation as measurement references, and no external reference base is needed. There is a high integration between inertial sensors and vehicle-mounted theodolites. Inertial sensor accuracy verification showed that the measurement error of the inertial sensor was less than 4″. However, over a long time, the measurement result of the twist angle could be degraded by gyro drift. The dual-axis inclinometer is also only capable of quasi-static roll angle and pitch angle measurements due to the hysteresis of the measurement data.

Yu et al. [25, 26] proposed a camera videometric measurement method to convert an unstable measuring platform to a static reference to solve the problems of large error or invalidation caused by measuring platform instability. This method installs a camera on the unstable platform and captures images of a reference marker fixed on a static reference or vice versa to resolve the 3D pose variation of the unstable platform relative to the static reference. The 3D pose variation represents the platform wobble errors in twist angle, roll angle and pitch angle. Liu et al. [27-29] and Liu et al. [30] achieved attitude measurement of a vehicle-mounted platform and a spacecraft tracking, telemetry, and control ship by using the camera videometric measurement method, respectively. In the meantime, the target body wobble errors were obtained. After applying wobble errors correction, the azimuth and pitch pointing angle of a theodolite on an unstable platform were substantially corrected. Zhang et al. [31] measured that the sensitivity of a vehicle-mounted platform attitude measurement was less than 3″ by using the camera videometric measurement method, and the correcting error was found to increase with increasing platform shaking amplitude. The correcting error was better than 16″ on the condition that the platform shaking amplitude was less than 13′. Nevertheless, the camera videometric measurement method takes a long time to perform the baseline calibration between the camera and the reference marker, which significantly limits the fast measuring characteristics of vehicle-mounted theodolites.

Zhang et al. [32] presented an optical self-collimation measurement method. The method installs a reflector on the vehicle-mounted platform and establishes a horizontal optical path between an external autocollimator and the reflector. Then, the shaking quantity of the vehicle-mounted platform is imaged on the charge coupled device (CCD) target surface in the autocollimator by light path transmission. The sensitivity of a vehicle-mounted platform attitude measurement depends on the pixel

angular resolution of the CCD target surface, which can usually reach 0.5″ or even 0.2″. Zhang et al. [33] measured, by using the optical self-collimation measurement method, that the maximal deformation of the azimuth and altitude are respectively 12.57″ and 5.98″ when the theodolite was guided at a speed of 60 °/s. Wang et al. [34] demonstrated through experimental tests that the optical self-collimation measurement method could compensate for the error from the deformation of the platform when working between ±0.7°, and the correcting error was better than 20″. Although the optical self-collimation measurement method is of high sensitivity, the establishment of the horizontal measurement reference also requires a long time as the measuring device is erected at a height of 1.4 m or more, and the establishment of the horizontal optical path lacks an adjustment reference. At the same time, the measurement of wobble angles in the pitch, roll and twist direction requires two sets of the measuring device vertically mounted.

Qiao et al. [35] provided a high-precision optical angular measurement method to measure the twist angle based on the moiré fringe produced by double diffraction grating interference. The twist angle deviation manifests itself as a change of the moiré fringe width, which in turn can measure the twist angle deviation by using the change of the moiré fringe width. The experimental result showed that based on the relationship between twist angle and moiré fringe, the measuring error was better than 0.2″ within the 7′ range compared with the 0.2″ autocollimator [36]. In addition, a dual-axis inclinometer was added for pitch and roll angle measurement, and a better correction effect was achieved. The error in the azimuth pointing angle is reduced from 129.691″ to 25.99″, and the error in the pitch pointing angle is reduced from 117.263″ to 27.82″ [37]. The measurement method can measure the twist angle with high precision, but the measuring device is capable of unidirectional wobble angle measurement only. The measurement of wobble angles in the pitch, roll and twist direction requires this method to be used in conjunction with other methods [38].

Wang et al. [39] presented an inclined measurement device with a photoelectric angle encoder and gravity hammer. This device can detect wobble angles in the pitch and roll direction by using a photoelectric angle encoder, respectively. Based on measured wobble angles, the incline in the theodolite coordinate system and the data of inclined angles are recorded through coordinate conversion. Finally, the azimuth and pitch pointing angle of the theodolite are corrected. The sensitivity of a vehicle-mounted platform attitude measurement depends on the angular accuracy of the photoelectric angle encoder, which can usually reach 2″ or even 1″. However, due to the limitation of the measuring principle, the device can detect wobble angles in the pitch and roll direction only. Meanwhile, higher equipment costs and structural modifications limit the applicability of this measurement method.

The above papers focus on how to realize the measurement of wobble error, as well as the measurement accuracy and correction effect. However, they lack the analysis of the operation convenience of the measuring device in calibration and preparation process, which is of non-negligible significance for the research on the wobble error measurement methods around engineering applications. In this paper, an auto-alignment non-contact optical measurement method for quantifying platform wobble error of a theodolite on a vehicle-mounted platform is proposed, which takes advantage of the feature that the vertical axis of the theodolite must be guaranteed to be perpendicular to the earth's horizontal plane when the theodolite works, and establishes the measurement optical path in the vertical direction. At the same time, a platform wobble error measuring device is designed, which can achieve automatic accurate alignment of the autocollimator and the reflector in 5 minutes and provides great convenience for rapid and accurate measurement of vehicle-mounted platform wobble errors. The proposed measurement method and the designed measuring device simultaneously take into account the measurement accuracy and the operation convenience, which are more promising for engineering applications than the existing models.

2 MEASUREMENT METHOD AND MODEL

2.1 Measurement Method

The vehicle-mounted platform wobble errors can be represented by a roll angle θ_x around the X axis, twist angle θ_y around the Y axis and pitch angle θ_z around the Z axis after establishing a geodetic coordinate system, as shown in Fig. 1. During the non-landing measurement of the theodolite, the vertical axis of the theodolite needs to be perpendicular to the ground. In addition, point positioning and azimuth/pitch pointing angle initialization also need to be completed. Then, the azimuth pointing angle A_Z and pitch pointing angle E_Z of the target can be obtained by using a photoelectric angle encoder. Here, θ_x, θ_y and θ_z with the same sequence of A_Z/E_Z can be obtained by using the platform wobble error measuring device. Finally, the master control computer finishes all data acquisition and correction of the target azimuth/pitch pointing angle. The correction method is the algebraic correction method based on the rigid body motion model that is mentioned in [23]. The correction process of the target azimuth/pitch pointing angle is shown in Fig. 2.

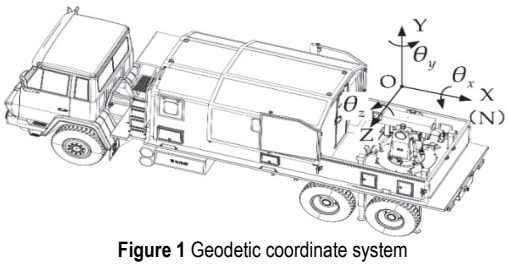

Figure 1 Geodetic coordinate system

The principle of the auto-alignment non-contact optical measurement method is shown in Fig. 3. The autocollimator is fixed vertically on the vehicle-mounted platform, and the reflector is placed on the ground as a relative reference. In the initial state, the platform can be automatically levelled by using the hydraulic or mechanical legs of automatic levelling mechanism, and the reflector also uses its own automatic levelling mechanism to automatically calibrate the reflecting surface level. The

automatic levelling of the platform and the reflector can ensure that the incident beam of the autocollimator automatically returns in the same way and images on the CCD target surface while the image point becomes the measuring reference point. Thus, an auto-alignment optical path in the vertical direction is established.

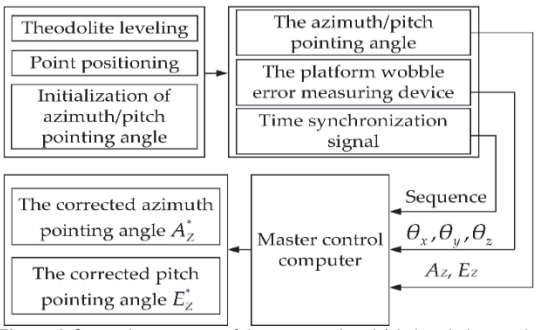

Figure 2 Correction process of the target azimuth/pitch pointing angle

During the non-landing measurement of the theodolite, the vehicle-mounted platform wobble errors cause direction changes in the incident beam and displacement of the image point. The image point deviation angle can be calculated by image point off-target interpretation. The relationship between the CCD image point deviation angle and image point displacement is as follows:

$$\begin{cases} \alpha_x = \Delta x \cdot \sigma / 2 \\ \alpha_z = \Delta z \cdot \sigma / 2 \end{cases} \tag{1}$$

Δx and Δz are the image point displacements relative to the base reference point, and σ represents the pixel angular resolution.

Since the CCD image point deviation angles are caused by the vehicle-mounted platform wobble errors θ_x, θ_y and θ_z, there exists a functional relation:

$$f\left(\theta_x, \theta_y, \theta_z\right) = Position\left(\alpha_x, \alpha_z\right) \tag{2}$$

Further, the establishment of an accurate expression ensures the solution of the vehicle-mounted platform wobble errors θ_x, θ_y and θ_z.

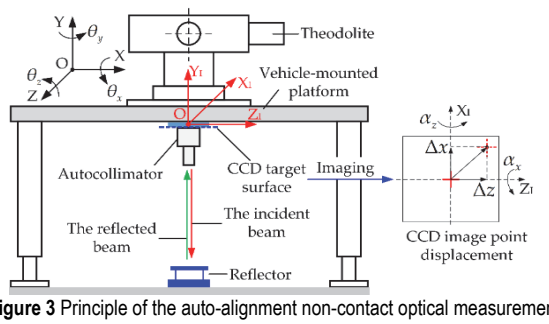

Figure 3 Principle of the auto-alignment non-contact optical measurement method

2.2 Platform Wobble Error Measurement Model

2.2.1 Measuring Device

The deviation angle of the image point on the CCD can characterize up to two directional wobble variations. Therefore, an appropriate measurement device needs to be designed to obtain θ_x, θ_y and θ_z, where θ_x, θ_y and θ_z are the roll angle, twist angle and pitch angle in the geodetic coordinate system. As shown in Fig. 4, two autocollimators are fixed on the platform at a certain angle and form a self-collimating optical path with reflectors. The vehicle-mounted platform is designed with a mounting interface for the theodolite and autocollimators to ensure the coordinate system overlap of O-XYZ, O-X′Y′Z′, O-$X_I Y_I Z_I$ and O-$X_{II} Y_{II} Z_{II}$ in the initial state.

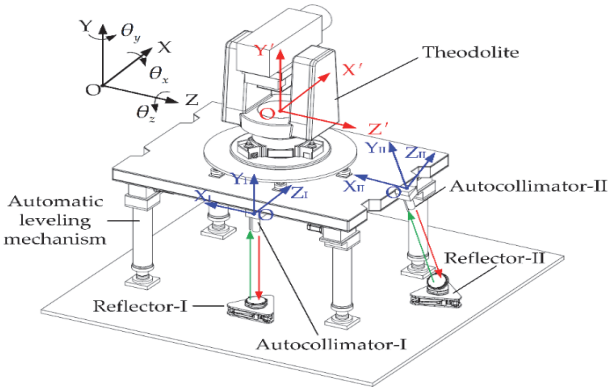

Figure 4 Platform wobble error measuring device

Autocollimator-I is fixed on the vehicle-mounted platform, and the incident beam is perpendicular to the ground. Reflector-I is placed on the ground as a relative reference with the reflecting surface parallel to the ground. Autocollimator-II is fixed on the vehicle-mounted platform with a slope angle θ_0. The slope angle between the reflecting surface of reflector-II and the horizontal plane is also θ_0.

Affected by the ground level, the theodolite needs to use an automatic levelling mechanism for the levelling of the vehicle-mounted platform when performing non-landing measurements. As reported in [40], the mainstream levelling mechanism currently used for vehicle-mounted platform levelling can achieve a plumbness error level of ≤ 30″. It is important to achieve automatic accurate optical path alignment of the measuring device and accurate measurement of the wobble errors.

A 3D schematic of reflector-I and reflector-II is shown in Fig. 5. Due to the small field of view of the autocollimator, to ensure that the image point can be quickly and accurately imaged on the CCD target surface, reflector-I and reflector-II are designed with a wedge-type automatic levelling mechanism and a dual-axis inclinometer. Through timely detection of reflector tilt and automatic horizontal calibration, the incident beam and reflected beam can be quickly and automatically adjusted to the autocollimator view field and display imaging on the CCD target surface.

In addition, to ensure the accurate alignment of reflector-II and autocollimator-II, reflector-II is designed with a rotating shaft with a lock valve, which is used to achieve axial rotation locking and positioning. At the same time, reflector-I and reflector-II can be adjusted timely to avoid tilt error caused by temperature, which improves the environmental adaptability of the vehicle-mounted platform wobble error measuring device.

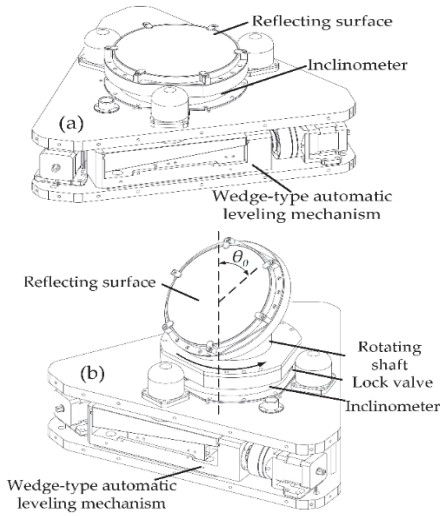

Figure 5 Reflector model: (a) Reflector-I; (b) reflector-II

2.2.2 Mathematical Model

A mathematical model of the platform wobble error measurement is established by using the ray-tracing method, as shown in Fig. 6. In the initial state, the coordinate systems of O-XYZ, O-$X_IY_IZ_I$ and O-$X_{II}Y_{II}Z_{II}$ maintain overlap relationship, where the OX axis is parallel and in the same direction with the OZ_I axis, the OZ axis is parallel and in the opposite direction with the OX_I axis. Moreover, there is a slope angle θ_0 between the OX axis and the OZ_{II}, and the OZ axis is parallel and in the opposite direction with the OX_{II} axis. As the geodetic coordinate system, the coordinate system of O-XYZ is constant while the coordinate systems of O-$X_IY_IZ_I$ and O-$X_{II}Y_{II}Z_{II}$ generate spatial motion with the platform.

Since the platform wobble considers only the angular wobble in the three directions of θ_x, θ_y and θ_z, the point displacement is ignored. Therefore, it can be assumed that the CCD-I target surface OX_IZ_I and the CCD-II target surface $OX_{II}Z_{II}$ always transform spatially around the reference point O.

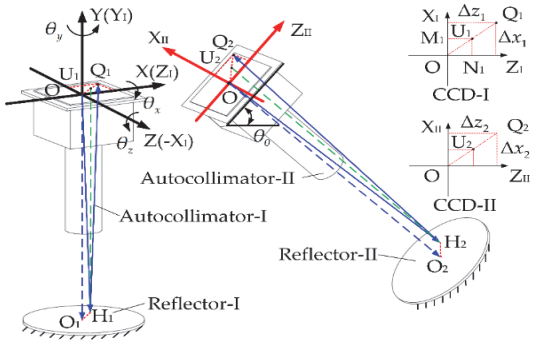

Figure 6 Geometric model

The rotation matrix R_x, R_y, R_z can be expressed as:

$$R_x = \begin{bmatrix} 1 & 0 & 0 \\ 0 & \cos\theta_x & -\sin\theta_x \\ 0 & \sin\theta_x & \cos\theta_x \end{bmatrix} \tag{3}$$

$$R_y = \begin{bmatrix} \cos\theta_y & 0 & \sin\theta_y \\ 0 & 1 & 0 \\ -\sin\theta_y & 0 & \cos\theta_y \end{bmatrix} \tag{4}$$

$$R_z = \begin{bmatrix} \cos\theta_z & -\sin\theta_z & 0 \\ \sin\theta_z & \cos\theta_z & 0 \\ 0 & 0 & 1 \end{bmatrix} \tag{5}$$

Assuming that the rotation order is *Y*, *Z* and *X* axes, then the transformation matrix of any point can be expressed as:

$$R_{xzy} = R_x R_z R_y = \begin{bmatrix} R_1 & R_4 & R_7 \\ R_2 & R_5 & R_8 \\ R_3 & R_6 & R_9 \end{bmatrix} \tag{6}$$

where R_1, R_2, R_3, R_4, R_5, R_6, R_7, R_8 and R_9 are the elements in the matrix of R_{xzy}, and they can be obtained by using Eq. (3), Eq.(4), Eq. (5) and Eq. (6).

Based on the spatial plane equation and the angular wobble in the three directions of θ_x, θ_y and θ_z, the equation of the CCD-I target surface OX_IZ_I in the geodetic coordinate system can be expressed as:

$$R_4 X + R_5 Y + R_6 Z = 0 \tag{7}$$

where *X*, *Y* and *Z* are the coordinate values in the geodetic coordinate system. Then, the equations of the spatial lines OX_I, OZ_I, OH_1, H_1U_1, U_1M_1 can be obtained by the spatial geometric relations.

In order to calculate the deviation angle by using the geometric model, supposing the initial distance between the CCD-I target surface OX_IZ_I and the reflecting surface of reflector-I is h_0. Based on the distance formula from the point to the straight line in 3D space, the coordinate value of meeting point M_1 in the coordinate system O-$X_IY_IZ_I$ can be expressed as:

$$\begin{bmatrix} X_1^* & Y_1^* & Z_1^* \end{bmatrix}^T = \begin{bmatrix} \dfrac{\sin\theta_x h_0}{\cos^2\theta_x \cos\theta_z} & 0 & 0 \end{bmatrix}^T \tag{8}$$

The deviation angle α_{1x} measured in the OX_I direction follows the equation:

$$\tan\alpha_{1x} = \frac{X_1^*}{|OH_1|} \tag{9}$$

Where:

$$|OH_1| = \frac{h_0}{\cos\theta_x \cos\theta_z} \tag{10}$$

Therefore, the relationship between α and θ_x can be obtained by using Eq. (8), Eq. (9) and Eq. (10):

$$\alpha_{1x} = \theta_x \tag{11}$$

Using the same derivation procedure as solving the relationship between α_{1x} and θ_x, the relationship between α_{1z} and θ_z can be obtained by the following equation:

$$\alpha_{1z} = \theta_z \tag{12}$$

From Eq. (11) and Eq. (12), autocollimator-I can directly measure θ_x and θ_z. The coupling relationship caused by θ_x, θ_y and θ_z does not have any effect on the angle measured by autocollimator-I.

2.2.3 Optimal Slope Angle Between Autocollimators

Due to the limitations of the CCD target size and pixel angular resolution, the cross wire twist attitude on the CCD target surface caused by θ_y cannot be solved with second-level accuracy according to off-target interpretation. Therefore, it is impossible to use autocollimator-I to achieve a second-level accuracy measurement of θ_y, and a combined measurement with autocollimator-II is required for the solution of θ_y.

When the platform is at twist angle θ_y, deviation angles α_{2x}, α_{2z} are obtained in the OX_{II} and OZ_{II} directions because of the slope angle θ_0. The initial state equation of the CCD-II target surface $OX_{II}Z_{II}$ in the geodetic coordinate system is:

$$\cos\theta_0 \cdot \mathrm{Y} - \sin\theta_0 \cdot \mathrm{X} = 0 \tag{13}$$

Since the deviation angle is independent of the measured distance, supposing the initial distance between the CCD-II target surface $OX_{II}Z_{II}$ and the reflecting surface of reflector-II is also h_0; then, the initial state reflecting surface equation of reflector-II can be calculated by Eq. (14):

$$\cos\theta_0 \cdot \mathrm{Y} - \sin\theta_0 \cdot \mathrm{X} + \mathrm{h}_0 = 0 \tag{14}$$

Using the same derivation procedure as shown in Section 2.2.2, when the platform is at angle θ_z only, the pitch angle θ_z can be directly measured in the OZ_{II} direction, and θ_z is unrelated to θ_0. However, when the platform is at angle θ_x only, the following equations can be obtained:

$$\begin{cases} \alpha_{2x} = \arctan\left(\dfrac{\sin\theta_0\sin\theta_x}{\sin^2\theta_0 + \cos^2\theta_0\cos\theta_x}\right) \\ \alpha_{2z} = \arctan\left(\dfrac{(1-\cos\theta_x)\sin\theta_0\cos\theta_0}{\sin^2\theta_0 + \cos^2\theta_0\cos\theta_x}\right) \end{cases} \tag{15}$$

When the platform is at angle θ_y only, the following equations can be obtained:

$$\begin{cases} \alpha_{2x} = \arctan\left(\dfrac{\sin\theta_0\sin\theta_y}{\cos^2\theta_0 + \sin^2\theta_0\cos\theta_y}\right) \\ \alpha_{2z} = \arctan\left(\dfrac{(1-\cos\theta_y)\sin\theta_0\cos\theta_0}{\cos^2\theta_0 + \sin^2\theta_0\cos\theta_y}\right) \end{cases} \tag{16}$$

Based on Eq. (16), the variation curves of α_{2x} and α_{2z} caused by θ_y and θ_0 can be obtained, as shown in Fig. 7. From the variation curve of Fig. 7a, the deviation angle α_{2x} varies significantly with different values of θ_y and θ_0. The variation magnitude is approximately 1×10^{-1} (°). The variation curve of Fig. 7b shows that deviation angle α_{2z} varies with different values of θ_y and θ_0. The variation magnitude is approximately 1×10^{-4} (°).

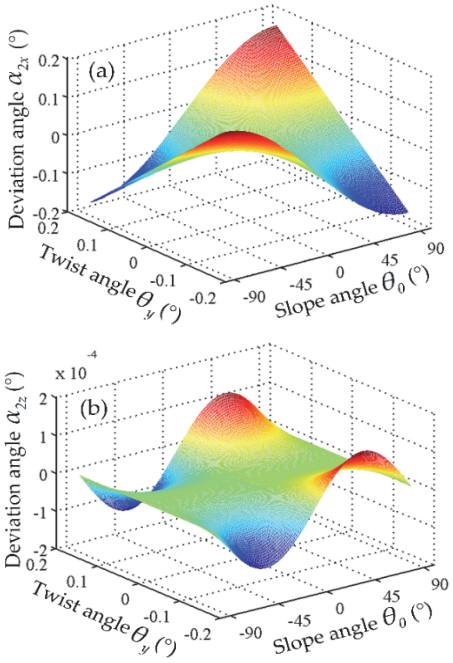

Figure 7 Variation curves of the deviation angle caused by θ_y and θ_0: (a) Variation curve of α_{2x}; (b) variation curve of α_{2z}

Assuming that $\theta_y = 10'$, the variation curves of α_{2x} and α_{2z} caused by θ_0 can be obtained, as shown in Fig. 8. From Fig. 8a, the deviation angle α_{2x} varies significantly with different values of θ_0 and reaches the extreme value when $\theta_0 = \pm 90^\circ$. From Fig. 8b, the deviation angle α_{2z} reaches the extreme value when $\theta_0 = \pm 45^\circ$. The variation curves of α_{2x} and α_{2z} caused by θ_y and θ_0 can also be obtained based on Eq. (15), which is the same situation as in Fig. 7 and Fig. 8.

Although the image point moves in the OX_{II} direction with the highest sensitivity when $\theta_0 = \pm 90^\circ$, the autocollimator-II incident beam is level with the horizontal

plane, and the reflecting surface of reflector-II should be perpendicular to the horizontal plane. This leads to problems with the erection and leveling of reflector II and loses its ease of operation. When setting up the measuring device, the slope angle θ_0 is finally chosen to be 45°.

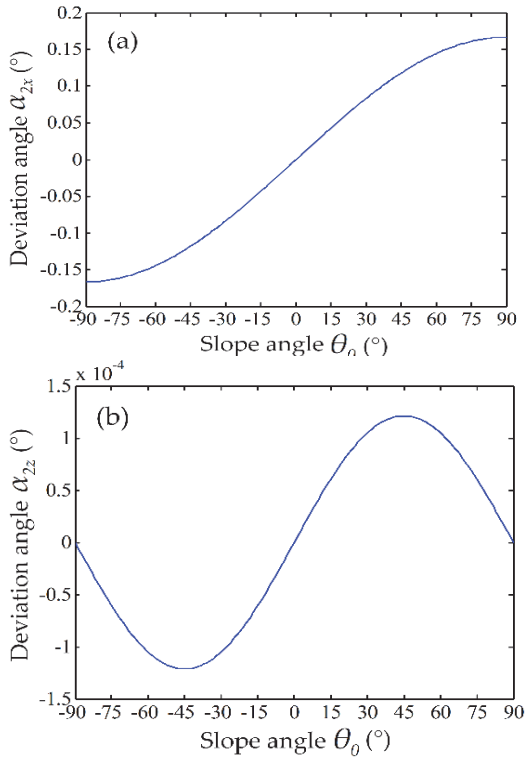

Figure 8 Variation curves of the deviation angle caused by θ_0 ($\theta_y = 10'$): (a) Variation curve of α_{2x}; (b) variation curve of α_{2z}

2.2.4 Approximate Analytical Equations of θ_y

The initial state equation of the CCD-II target surface $OX_{II}Z_{II}$ can be expressed as:

$$Y - X = 0 \tag{17}$$

When the platform is at θ_x, θ_y and θ_z, the following equation can be obtained:

$$(R_1 - R_4)X + (R_2 - R_5)Y + (R_3 - R_6)Z = 0 \tag{18}$$

Since θ_x and θ_z are obtained by using autocollimator-I, it is possible to define Eq. (18) as a function of θ_y. Based on the same derivation process, after neglecting the higher order minima and simplifying the equations, the approximate analytical equations for α_{2x}, α_{2z} and θ_y can be written as:

$$\alpha_{2x} \approx \arctan\left(\frac{R_d\left(R_b\sin\theta_y - R_a\right)}{R_b\cos\theta_y + R_a\sin\theta_y - R_c}\right) \tag{19}$$

$$\alpha_{2z} \approx \arctan\left(\frac{\sqrt{2}R_d\left(R_a\sin\theta_y + R_b + R_c\cos\theta_y\right)}{2\left(R_b\cos\theta_y + R_a\sin\theta_y - R_c\right)}\right) \tag{20}$$

Where:

$$\begin{cases} R_a = (\sin\theta_z - \cos\theta_z)\sin\theta_x \\ R_b = \sin\theta_z + \cos\theta_z \\ R_c = (\sin\theta_z - \cos\theta_z)\cos\theta_x \\ R_d = \sqrt{R_b^2 + R_c^2} \end{cases} \tag{21}$$

Assuming that $\theta_x = \theta_z = 6'$, the variation curves of α_{2x} and α_{2z} caused by θ_0 can be obtained by using Eq. (19) and Eq. (20), as shown in Fig. 9. Notably, α_{2x} varies approximately linearly with the same magnitude as θ_y, while α_{2z} varies almost invariably with θ_y. Hence, Eq. (19) is used for the calculation of θ_y, thus eliminating the redundancy of equations in the simultaneous calculation of θ_y by using Eq. (19) and Eq. (20).

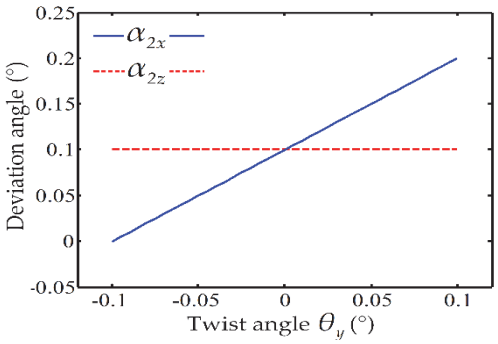

Figure 9 Variation curves of the deviation angle caused by θ_y

3 EXPERIMENTS AND RESULTS

3.1 Test Platform Composition

The vehicle-mounted theodolite can be divided into two parts: the electro-optical theodolite and automatic levelling mechanism, as shown in Fig. 10a. A visible light measurement module is installed on the electro-optical theodolite with focal length 4000 mm, primary mirror diameter 400 mm, image element resolution 1920 × 1080, image element size 10 μm × 10 μm, and pixel angular resolution 0.51″. The automatic levelling mechanism includes a vehicle-mounted platform, four mechanical levelling legs, a dual-axis inclinometer and a levelling control module. The dual-axis inclinometer is a BWS2800-I with a quasistatic accuracy of 0.001° made by BWSENSING, and the specific parameters are shown in Tab. 1.

The platform wobble error measuring device is shown in Fig. 10b to Fig. 10d. The autocollimator is a TA200-38 with an accuracy of 1.3″ made by TRIOPTICS, and the specific parameters are shown in Tab. 2. The mirror diameters of reflector-I and reflector-II are 200 mm, and the surface figure error is less than 31.64 nm. The dual-axis inclinometer is also a BWS2800-I.

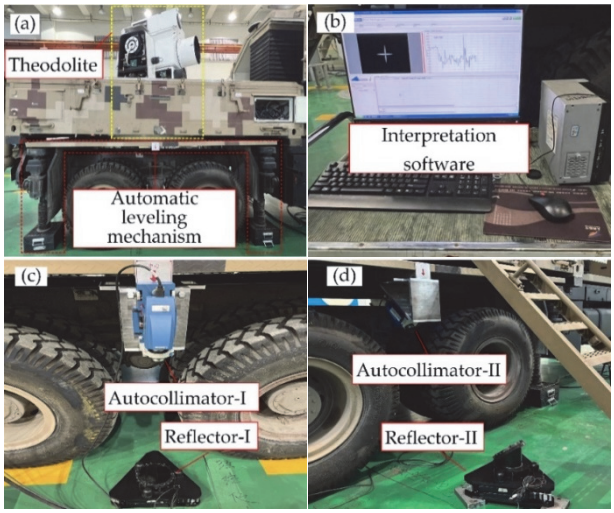

Figure 10 Test platform composition: (a) Vehicle-mounted theodolite; (b) interpretation software; (c) autocollimator-I & reflector-I; (d) autocollimator-II & reflector-II

Table 1 BWS2800-I parameters

Parameter	Measuring condition	Value
measuring range / °	horizontal plane	±5
measuring axis	mutual vertical	*X* - *Y*
accuracy / °	room temperature	0.001
resolution / °	static	0.0005
zero-point temperature drift / °/°C	−40 ~ 85 °C	±0.0007
cross-axis error / °	−40 ~ 85 °C	0.001
output frequency / Hz	5 ~ 100 Hz	≤ 100

Table 2 TA200-38 parameters

Parameter	Value
focal length / mm	200
transmission aperture / mm	30
field of view / ″	3090 × 2470
resolution / ″	0.05
repeatability accuracy / ″	±0.12
accuracy / ″	±1.3

3.2 Pointing Accuracy Experiment

The relative angle between the horizontal parallel light pipe and the high-angle parallel light pipe is statically calibrated by using a total station. The total station is a Leica TS60 made by Leica Camera AG, which has a goniometric accuracy of 0.5″. The true relative angle values of the azimuth and pitch are respectively ΔA_R and ΔE_R. In the stationary state of the vehicle-mounted platform, the azimuth and pitch angles are respectively A_0 and E_0 as measured by the horizontal parallel light pipe, and the azimuth and pitch angles are respectively A_{Z0} and E_{Z0} as measured by the high-angle parallel light pipe. The static azimuth and pitch pointing angles of the vehicle-mounted theodolite can be obtained:

$$\begin{cases} \Delta A_{Z0} = A_{Z0} - A_0 \\ \Delta E_{Z0} = E_{Z0} - E_0 \end{cases} \tag{22}$$

The static azimuth and pitch pointing angle errors can be calculated as follows:

$$\begin{cases} \Delta A_{D0} = \Delta A_R - \Delta A_{Z0} \\ \Delta E_{D0} = \Delta E_R - \Delta E_{Z0} \end{cases} \tag{23}$$

The static azimuth and pitch pointing angle errors with 50 sets of tests are given in Fig. 11. According to the statistics, the average errors of the static azimuth and pitch pointing angle are respectively 6.8″ and 9.1″, and the standard deviations are all 0.1″. Therefore, the average errors of the static azimuth and pitch pointing angle can be used as a data comparison benchmark.

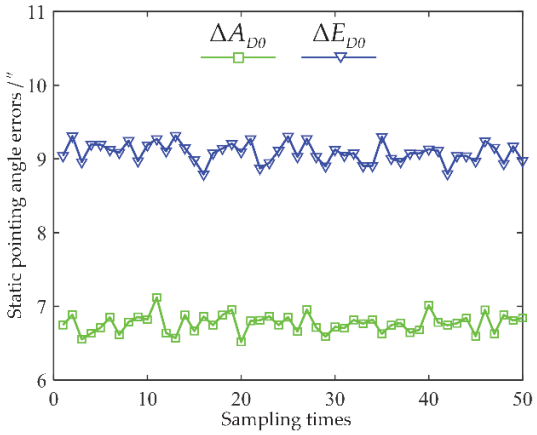

Figure 11 Data presentation of the static azimuth and pitch pointing angle errors

With A_{Z0} and E_{Z0} as the initial position, the theodolite measures the high-angle parallel light pipe dynamically according to the angular motion path shown in Eq. (24), which ensures that the theodolite has a maximum angular acceleration of 25 $^{\circ}/\mathrm{s}^2$ when its optical axis is pointing to the high-angle parallel light pipe. Meanwhile, the vehicle-mounted platform has the maximum wobble error. The maximum angular velocity of the theodolite is 35 $^{\circ}/\mathrm{s}^2$.

$$\begin{cases} A_{\Delta} = 49\cos(0.7143 \cdot t) \\ E_{\Delta} = 49\cos(0.7143 \cdot t) \end{cases} \tag{24}$$

where A_{Δ} is the azimuth angle with A_{Z0} taken as a reference (unit: °); E_{Δ} is the pitch angle with E_{Z0} taken as a reference (unit: °); and t is the measuring time (unit: s). When the theodolite sweeps through the high-angle parallel light pipe, A_{Zi}, E_{Zi}, α_{1xi}, α_{1zi} and α_{2xi} can be obtained, corresponding to the sampling sequence i. Furthermore, based on Eq. (11), Eq. (12) and Eq. (19), the platform wobble errors θ_{xi}, θ_{yi} and θ_{zi} can be calculated. The data curves of α_{1xi}, α_{1zi} and α_{2xi} collected by the platform wobble error measuring device and the calculated data curve θ_{yi} are shown in Fig. 12.

The theodolite performs a sine cycle oscillation in the experiment. Therefore, the theodolite can repeatedly sweep to the high-angle parallel light pipe several times and obtain multiple sets of experimental test data approximating the sinusoidal curve. After acquiring multiple sets of images of the high-angle parallel light pipe

through the experiment, the azimuth and pitch angles corresponding to the shape centers of the images are extracted using the interpretation software. The sampling positions P1 ~ P6 shown in Fig. 12b are the position where the optical axis is pointing to the high-angle parallel light pipe, which corresponds to the maximum of θ_{xi}, θ_{yi} and θ_{zi}.

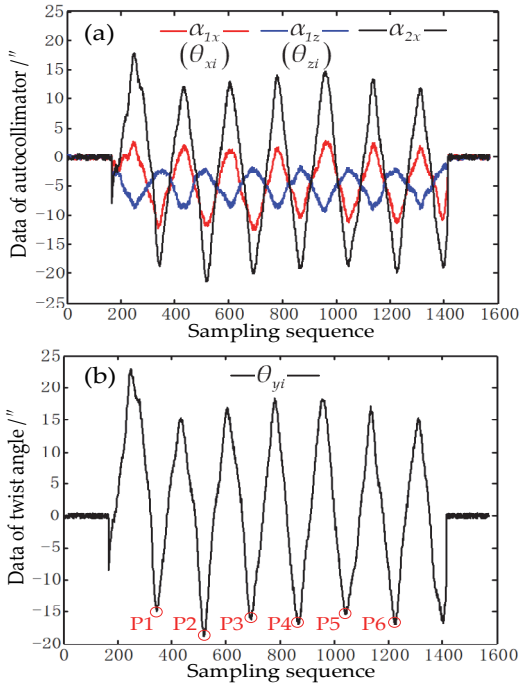

Figure 12 Data presentation of the measurement results of the experiment: (a) Autocollimator data; (b) twist angle data

Therefore, the data at this sampling point are used to analyze the correction of the theodolite's dynamic azimuth and pitch pointing angle, and the corrected relationship between A_{Zi}^{*}, E_{Zi}^{*} and A_{Zi}, E_{Zi} is shown in Eq. (25), and the corresponding correction results are shown in Tab. 3.

$$\begin{cases} A_{Zi}^{*} = \arctan\dfrac{R_3R_{ei} + R_6R_{fi} + R_9R_{gi}}{R_1R_{ei} + R_4R_{fi} + R_7R_{gi}} \\ E_{Zi}^{*} = \arcsin\left(R_2R_{ei} + R_5R_{fi} + R_8R_{gi}\right) \end{cases} \tag{25}$$

Where:

$$\begin{cases} R_{ei} = \cos E_{Zi}\cos A_{Zi} \\ R_{fi} = \sin E_{Zi} \\ R_{gi} = \cos E_{Zi}\sin A_{Zi} \end{cases} \tag{26}$$

In order to reduce the randomness of experimental test error, 19 sets of tests are repeated according to the same angular motion path, and the data at sampling positions P7 ~ P120 are obtained. Then, the variation curves of the platform wobble errors and the dynamic pointing angle errors are given in Fig. 13. According to the statistics, the average errors of θ_{xi}, θ_{yi} and θ_{zi} are respectively −11.2″, −16.5″ and −2.3″, and the standard deviations are respectively 0.55″, 1.29″ and 0.34″. Meanwhile, the average errors of ΔA_{Di}, ΔE_{Di}, ΔA_{Di}^{*} and ΔE_{Di}^{*} are respectively 31.5″, 21″, 9.8″ and 9.2″, and the standard deviations are respectively 2.01″, 1.71″, 1.69″ and 1.89″. Influenced by the calibration error of the measuring device, point extraction noise of the interpretation software, the stiffness of the theodolite and the support stability of automatic levelling mechanism, the standard deviation data obtained is much larger when the theodolite is under the sine cycle oscillation.

Table 3 Correction of the theodolite's azimuth and pitch pointing angle

Parameter	P1	P2	P3	P4	P5	P6
θ_{xi} / ″	−10.8	−11.3	−11.8	-10.2	−10.5	−11.3
θ_{yi} / ″	−15	−18.8	−15.4	-16.3	−14.4	−17
θ_{zi} / ″	−2.8	−2.3	−2.3	−2.2	−2.1	−2.1
A_{Zi} / °	114.344	114.3434	114.3424	114.3442	114.3428	114.3432
E_{Zi} / °	65.5985	65.5984	65.5967	65.5973	65.5978	65.5979
A_{Zi}^{*} / °	114.3493	114.3502	114.3484	114.3501	114.3483	114.3496
E_{Zi}^{*} / °	65.6016	65.6015	65.5999	65.6001	65.6007	65.6010
ΔA_{Zi} / °	82.8345	82.8339	82.8329	82.8347	82.8333	82.8337
ΔE_{Zi} / °	65.7258	65.7257	65.7240	65.7246	65.7251	65.7252
ΔA_{Zi}^{*} / °	82.8398	82.8407	82.8389	82.8406	82.8388	82.8401
ΔE_{Zi}^{*} / °	65.7289	65.7288	65.7272	65.7274	65.7280	65.7283
ΔA_{Di} / ″	29.9	32.0	35.6	29.2	34.2	32.8
ΔE_{Di} / ″	18.0	18.4	24.5	22.3	20.5	20.2
ΔA_{Di}^{*} / ″	10.7	7.6	14.1	8.0	14.5	9.7
ΔE_{Di}^{*} / ″	7.0	7.1	12.8	12.1	10.1	9.0

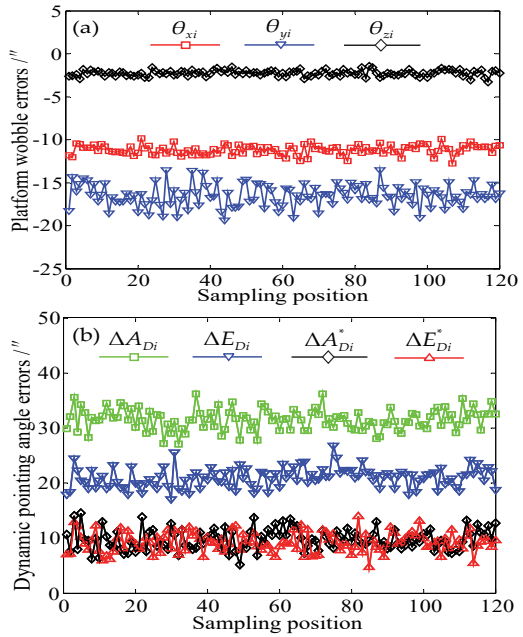

Figure 13 Data presentation of the measurement results at sampling positions P1 ~ P120: (a) Platform wobble errors data; (b) dynamic pointing angle errors data

The differences between the average errors of the dynamic azimuth and pitch pointing angle without correction and the static one reach 24.7″ and 11.9″ respectively, which reveals that the platform wobble error has a significant effect on the dynamic azimuth and pitch pointing angle accuracy of the theodolite. However, the differences between the average errors of the dynamic azimuth and pitch pointing angle with correction and the static one only have 3″ and 0.1″ respectively. The 3σ accuracy of the dynamic azimuth and pitch pointing angle with correction only have 8.07″ and 5.77″ respectively. But without correction, the 3σ accuracy of the dynamic azimuth and pitch pointing angle reach 30.73″ and 17.03″ respectively. The dynamic azimuth and pitch pointing angle accuracy of the theodolite have been significantly improved, which demonstrates the realizability of the measurement of wobble error, as well as the measurement accuracy and correction effect.

4 DISCUSSION

During the non-landing measurement of the theodolite, the vertical axis of the theodolite needs to be perpendicular to the ground. Therefore, a levelling test of the automatic levelling mechanism is carried out for the vehicle-mounted platform. Fig. 14a shows the angle measurement data collected by the dual-axis inclinometer during the levelling process of the automatic levelling mechanism. The *X*-direction tilt of the vehicle-mounted platform in the initial state is approximately 3000″, and the *Z*-direction tilt is approximately 1100″. Through levelling by an automatic levelling mechanism, the *X*-directional tilt is reduced to 16.6″, and the *Z*-directional tilt is reduced to 28.2″. Since the sampling frequency of the dual-axis inclinometer is selected as 100 Hz, it can be calculated that the total time spent from the extension of four legs to the completion of automatic levelling is approximately 5 minutes.

Furthermore, an automatic levelling experiment is conducted on the reflector. As the reflector needs to be adjusted to second-level accuracy, the frequency of the dual-axis inclinometer is reduced, and the sampling frequency is set to 10 Hz. As shown in Fig. 14b, the initial tilt of the *X*-direction and *Z*-direction is approximately 1800″, the *X*-direction tilt is reduced to 2.6″, and the *Z*-direction tilt is reduced to 0.8″ after approximately 2 minutes of levelling. The experimental result shows that the reflector under automatic levelling automatically returns the incident beam to the field of view of the autocollimator, which shows that the measuring device can achieve an auto-alignment optical path for the measurement of the platform wobble error.

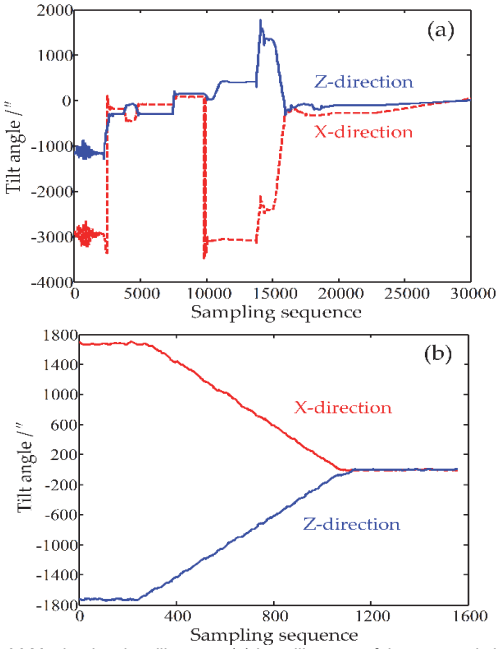

Figure 14 Mechanism levelling test: (a) Levelling test of the automatic leveling mechanism; (b) levelling test of the reflector

TA200-38 has a field of view of 3090 × 2470 (unit: ″), so under the condition of high-precision levelling of the automatic levelling mechanism and reflector, it is extremely easy to realize accurate auto-alignment of the autocollimator and the reflector, which provides great convenience for rapid and accurate measurement of vehicle-mounted platform wobble errors.

The measuring device designed in this paper does not need to be calibrated for a long time and can better meet the needs of vehicle-mounted theodolites for motorized measurements. However, the experiments conducted in the paper are under indoor environment, and the experiments considering wind loads and temperature variation have not been conducted. Therefore, verifying the environmental suitability of the measurement device will be one of the most important tasks in the future. At the same time, the correction effect for the azimuth and pitch pointing angle of vehicle-mounted theodolites under multiple perturbations also needs to be verified.

5 CONCLUSIONS

An auto-alignment non-contact optical measurement method was proposed in this paper to measure the roll angle, twist angle and pitch angle of the platform. With automatic levelling, the corresponding measuring device

established an auto-alignment optical path in the vertical direction within 5 minutes and achieved the measurement of the platform wobble error with high precision. The experiment result showed that, after the measurement of the platform wobble errors based on the proposed measurement method and the designed measuring device, the average errors of the dynamic azimuth and pitch pointing angle with correction were 9.8″ and 9.2″ respectively, which is close to the static result of 6.8″ and 9.2″. This result fully highlights the substantial correction effect achieved by the proposed method.

The proposed measurement method and the designed measuring device are an important complement to the field of the platform wobble error measurement. In comparison with other methods, the establishment of the measurement reference optical path is rapidly realized by using automatic levelling mechanism, without manual involvement. The operation convenience of the measuring device reflected in calibration and preparation process, which was presented in the paper, would make the proposed measurement method more promising for engineering applications. It could be directly applied to the field of shaking measurement of various unstable platforms and micro-vibration measurement of tiny structure in the future.

Acknowledgements

This work was supported by the National Natural Science Foundation of China (Grant No. 12103081).

6 REFERENCES

[1] Wilson, K. E., Britcliffe, M., & Golshan, N. (2000). Progress in design and construction of the Optical Communications Telescope Laboratory (OCTL). *Proceedings of the Free-Space Laser Communication Technologies XII*, San Jose, United States, 2 May 2000, 112-116. https://doi.org/10.1117/12.384302

[2] Yakimenko, O. A., Tiaden, R. D., & Berlind, R. M. (2008). Payload derived position and attitude acquisition system for parachute recovery systems. *Proceedings of the 2008 16th Mediterranean Conference on Control and Automation, Ajaccio*, France, 25-27 June 2008, 1198-1203. https://doi.org/10.1109/MED.2008.4601976

[3] Paar, R., Marendić, A., Jakopec, I., & Grgac, I. (2021). Vibration Monitoring of Civil Engineering Structures Using Contactless Vision-Based Low-Cost IATS Prototype. *Sensors 21*, 7952. https://doi.org/10.3390/s21237952

[4] Tang, Y. & Zhang, P. (2022). The Impact of virtual integration on innovation speed: on the view of organizational information processing theory. *Journal of Organizational and End User Computing*, *34*, 1-20. https://doi.org/10.4018/JOEUC.298702

[5] Prel, F., Moreau, L., Bouchard, R., Bullis, R. D., Roy, C., Vallières, C., & Levesque, L. (2013). Hyperspectral imaging spectro radiometer improves radiometric accuracy. *Proceedings of the Infrared Imaging Systems: Design, Analysis, Modeling, and Testing XXIV*, Baltimore, United States, 5 June 2013, 249-260. https://doi.org/10.1117/12.2017688

[6] Prel, F., Moreau, L., Lantagne, S., Bullis, R. D., Roy, C., Vallières, C., & Levesque, L. (2012). Infrared signature measurements with the ABB dual-band hyperspectral imager. *Proceedings of the Infrared Imaging Systems: Design, Analysis, Modeling, and Testing XXIII*, Baltimore, United States, 18 May 2012, 283-293. https://doi.org/10.1117/12.918686

[7] Prel, F., Moreau, L., Lantagne, S., Bullis, R. D., Roy, C., Vallières, C., & Levesque, L. (2011). MRi dual-band MWIR imaging FTS. *Proceedings of the Infrared Imaging Systems: Design, Analysis, Modeling, and Testing XXII*, Orlando, United States, 9 May 2011, 360-369. https://doi.org/10.1117/12.883536

[8] Xie, X. & Peng, Y. (2022). Data Asset Management and Visualization Based on Intelligent Algorithm: Taking Power Equipment Data as An Example. *Tehnički vjesnik*, *29*, 1109-1119. https://doi.org/10.17559/TV-20220410150901

[9] Chen, H., Ge, J., Kong, D., Zhao, Z., & Zhu, Q. (2022). A Real-Time Monitoring Method for Civil Aircraft Take-Off and Landing Based on Synthetic Aperture Microwave Radiation Technology. *Sensors*, *22*, 3675. https://doi.org/10.3390/s22103675

[10] Wang, T. (2021). A K-means group division and LSTM based method for hotel demand forecasting. *Tehnički vjesnik*, *28*, 1345-1352. https://doi.org/10.17559/TV-20210507172841

[11] Merritt, P. H. & Albertine, J. R. (2013). Beam control for high-energy laser devices. *Optical Engineering*, *52*, 021005. https://doi.org/10.1117/1.OE.52.2.021005

[12] Smith, C. R., Grasso, R., Pledger, J., & Murarka, N. (2012). Trends in electro-optical electronic warfare. *Proceedings of the Technologies for Optical Countermeasures IX*, Edinburgh, United Kingdom, 14 November 2012, 854302. https://doi.org/10.1117/12.978652

[13] Lu, C., Yin, J., & Wu, H. (2022). A Hierarchical Clustering Federated Learning System Based on Industry 4.0. *Journal of Organizational and End User Computing*, *34*, 1-16. https://doi.org/10.4018/JOEUC.313194

[14] Ruffatto, D., Brown, D., Pohle, R., Reiley, M., & Haddock, D. (2001). Stabilized high-accuracy optical tracking system (SHOTS). *Proceedings of the Acquisition, Tracking, and Pointing XV*, Orlando, US, 21 August 2001, 10-18.

[15] Harvey, J. E., Krywonos, A., & Houston Jr, J. B. (2005). Performance modeling of launch vehicle imaging telescopes. *Proceedings of the Optical Modeling and Performance Predictions II*, San Diego, United States, 18 August 2005, 125-136. https://doi.org/10.1117/12.626031

[16] Bai, X., Wang, Y., Gao, X., & Yu, Q. (2009). Research on measuring and modifying for mobile theodolite's sloshing. *Infrared and Laser Engineering*, *38*, C-0161-05.

[17] Li, Z., Wu, Z., Tong, G., & Chen, T. (2010). Pointing error correction for vehicular platform theodolite. *Optics and Precision Engineering*, *18*, 921-927.

[18] Yan, H., Liu, Y., & Wang, D. (2014). Correction method of dynamic error of optoelectronic theodolite. *Infrared and Laser Engineering*, *43*, 3030-3035.

[19] Jiang, B., Zhou, S., Jiang, K., Fu, H., & Mei, C. (2015). Analysis of vertical axis error of vehicular theodolite. *Infrared and Laser Engineering*, *44*, 1623-1627.

[20] Jiang, W., Gao, Y., Feng, D., & Chen, Z.(2009). Corrected error of base-plane for vehicle-borne photoelectric theodolite. *Acta Armamentarii*, *30*, 1638-1641.

[21] Li, Z., Wu, Z., Tong, G., & Chen, T. (2010). Pointing error correction for vehicular platform theodolite. *Optics and Precision Engineering*, *18*, 921-927.

[22] Filatov, Y. V., Pavlov, P. A., Velikoseltsev, A. A., & Schreiber, K. U. (2020). Precision Angle Measurement Systems on the Basis of Ring Laser Gyro. *Sensors*, *20*, 6930. https://doi.org/10.3390/s20236930

[23] Luo, J., Xu, P., Pan, N., Jiang, P., Li, X., & Zhang, H. (2019). Non-landing vehicle-mounted electro-optical theodolite deformation measurement method using inertial sensors. *Measurement Science and Technology*, *30*, 055103. https://doi.org/10.1088/1361-6501/ab0ac1

[24] Luo, J., Fan, Y., Jiang, P., He, Z., Xu, P., Li, X., Yang, W., Zhou, W., & Ma, S. (2020). Vehicle platform attitude estimation method based on adaptive Kalman filter and sliding window least squares. *Measurement Science and Technology*, *32*. https://doi.org/10.1088/1361-6501/abc5f8
[25] Yu, Q., Sun, X., Jiang, G., Liu, X., Zhang, X., Zhou, J., & Shang, Y. (2011). Relay camera videometrics based conversion method for unstable platform to static reference. *Science China Technological Sciences*, *54*, 1017-1023. https://doi.org/10.1007/s11431-011-4296-1
[26] Yu, Q., Shang, Y., Zhou, J., Zhang, X., & Li, L. (2009). Monocular trajectory intersection method for 3D motion measurement of a point target. *Science in China Series E: Technological Sciences*, *52*, 3454-3463. https://doi.org/10.1007/s11431-009-0239-5
[27] Liu, J., Zhang, X., Liu, H., Yuan, Y., Zhu, Z., & Yu, Q. (2013). Correction method for non-landing measuring of vehicle-mounted theodolite based on static datum conversion. *Science China Technological Sciences*, *56*, 2268-2277. https://doi.org/10.1007/s11431-013-5303-5
[28] Liu, J.; Zhang, X.; Liu, H.; Yuan, Y.; Zhu, Z.; Yu, Q. (2013). New method for camera pose estimation based on line correspondence. *Science China Technological Sciences*, *56*, 2787-2797. https://doi.org/10.1007/s11431-013-5361-8
[29] Liu, J. & Zhu, Z. (2013). The high-precision videometrics methods to determining absolute vertical benchmark. *Proceedings of the Eighth International Symposium on Precision Engineering Measurement and Instrumentation, Chengdu*, China, 31 January 2013, 589-595. https://doi.org/10.1117/12.2016984
[30] Liu, H., Sun, C., Zhang, Y., Liu, X., Liu, J., Zhang, X., & Yu, Q. (2015). Hull deformation measurement for spacecraft TT&C ship by Photogrammetry. *Science China Technological Sciences*, *58*, 1339-1347. https://doi.org/10.1007/s11431-015-5867-3
[31] Zhang, X., Liu, J., Liu, T., Du, B., & Feng, Z. (2015). Measuring and correcting method for shaking platform of vehicle-mounted theodolite. *SCIENTIA SINICA Technologica*, *45*, 471-475. https://doi.org/10.1360/N092014-00422
[32] Zhang, Y., Zhang, M., & Qiao, Y. (2003). Research of a CCD Laser Collimation System with High Precision. *Journal of Optoelectronics·Laser*, *14*, 168-170.
[33] Zhang, D., Shang, C., & Qiao, Y. (2005). The research of deformation measurement technology of vehicle flat in photoelectric theodolite. *LASER & INFRARED*, *35*, 435-437.
[34] Wang, T., Tang, J., & Song, L. (2012). Correction of the measuring error of vehicular photoelectric theodolite. *Infrared and Laser Engineering*, *41*, 1335-1338.
[35] Qiao, Y., Wang, C., Li, X., Gao, F., Li, B., & Li, Y. (2008). Measurement of torsion angular distortion based on Moiré fringe. *Optics and Precision Engineering*, *16*, 2132-2139.
[36] Cai, S., Liang, S., Ding, Z., & Qiao, Y. (2008). Auto-collimation angular measurement method based on moiré fringe. *Journal of Optoelectronics·Laser*, *19*, 1375-1377.
[37] Tong, G. & Wang, F. (2011). Analysis and correction for influence of vehicle platform deformation on measuring errors. *Optics and Precision Engineering*, *19*, 775-781. https://doi.org/10.3788/OPE.20111904.0775
[38] Yin, Y., Cai, S., & Qiao, Y. (2016). Design, fabrication, and verification of a three-dimensional autocollimator. *Applied Optics*, 55, 9986-9991. https://doi.org/10.1364/AO.55.009986
[39] Wang, T. & Song, L. (2012). Measurement error correction of vehicular theodolite. *Chinese Journal of Scientific Instrument*, *33*, 469-473.
[40] Guo, L., Tan, H., & Zeng, M. (2022). Design of Automatic Leveling Control System for Special Vehicle-mounted Platform. *Proceedings of the 2022 International Conference on Artificial Intelligence and Computer Information Technology (AICIT)*, Yichang, China, 16-18 September 2022, 1-5. https://doi.org/10.1109/AICIT55386.2022.9930164

Contact information:

Xiangyu LI
1) Key Laboratory of Space Precision Measurement Technology, Xi'an Institute of Optics and Precision Mechanics, Chinese Academy of Sciences, Xi'an, 710119, China;
2) University of Chinese Academy of Sciences, Beijing, 100049, China;
NO.17 Xinxi Road, New Industrial Park, Xi'an Hi-Tech Industrial Development Zone, Xi'an, 710119, Shaanxi, P. R. China
E-mail: lixiangyu@opt.ac.cn

Wei HAO
Key Laboratory of Space Precision Measurement Technology, Xi'an Institute of Optics and Precision Mechanics, Chinese Academy of Sciences, Xi'an, 710119, China;
NO.17 Xinxi Road, New Industrial Park, Xi'an Hi-Tech Industrial Development Zone, Xi'an, 710119, Shaanxi, P. R. China
E-mail: haowei@opt.ac.cn

Meilin XIE
Key Laboratory of Space Precision Measurement Technology, Xi'an Institute of Optics and Precision Mechanics, Chinese Academy of Sciences, Xi'an, 710119, China;
NO.17 Xinxi Road, New Industrial Park, Xi'an Hi-Tech Industrial Development Zone, Xi'an, 710119, Shaanxi, P. R. China
E-mail: xiemeilin6@163.com

Bo LIU
Key Laboratory of Space Precision Measurement Technology, Xi'an Institute of Optics and Precision Mechanics, Chinese Academy of Sciences, Xi'an, 710119, China;
NO.17 Xinxi Road, New Industrial Park, Xi'an Hi-Tech Industrial Development Zone, Xi'an, 710119, Shaanxi, P. R. China
E-mail: LB3L@sina.com

Bo JIANG
Key Laboratory of Space Precision Measurement Technology, Xi'an Institute of Optics and Precision Mechanics, Chinese Academy of Sciences, Xi'an, 710119, China;
NO.17 Xinxi Road, New Industrial Park, Xi'an Hi-Tech Industrial Development Zone, Xi'an, 710119, Shaanxi, P. R. China
E-mail: ilysay@opt.ac.cn

Tao LV
1) Key Laboratory of Space Precision Measurement Technology, Xi'an Institute of Optics and Precision Mechanics, Chinese Academy of Sciences, Xi'an, 710119, China;
2) University of Chinese Academy of Sciences, Beijing, 100049, China;
NO.17 Xinxi Road, New Industrial Park, Xi'an Hi-Tech Industrial Development Zone, Xi'an, 710119, Shaanxi, P. R. China
E-mail: lvtao@opt.ac.cn

Wei SONG
1) Key Laboratory of Space Precision Measurement Technology, Xi'an Institute of Optics and Precision Mechanics, Chinese Academy of Sciences, Xi'an, 710119, China;
2) University of Chinese Academy of Sciences, Beijing, 100049, China;
NO.17 Xinxi Road, New Industrial Park, Xi'an Hi-Tech Industrial Development Zone, Xi'an, 710119, Shaanxi, P. R. China
E-mail: songwei2016@opt.ac.cn

Ping RUAN
(Corresponding author)
Key Laboratory of Space Precision Measurement Technology, Xi'an Institute of Optics and Precision Mechanics, Chinese Academy of Sciences, Xi'an, 710119, China;
NO.17 Xinxi Road, New Industrial Park, Xi'an Hi-Tech Industrial Development Zone, Xi'an, 710119, Shaanxi, P. R. China
E-mail: ruanp@opt.ac.cn